ARTICLE

Virus-Enabled Silicon Anode for Lithium-Ion Batteries

Xilin Chen,[†] Konstantinos Gerasopoulos,[‡,§] Juchen Guo,[†] Adam Brown,[⊥] Chunsheng Wang,[†,*] Reza Ghodssi,[‡,§,∥] and James N. Culver[⊥]

[†]Department of Chemical and Biomolecular Engineering, [‡]Department of Materials Science and Engineering, [§]Institute for Systems Research, [⊥]Center for Biosystems Research, University of Maryland Biotechnology Institute, and [∥]Department of Electrical and Computer Engineering, University of Maryland, College Park, Maryland 20742

ABSTRACT A novel three-dimensional Tobacco mosaic virus assembled silicon anode is reported. This electrode combines genetically modified virus templates for the production of high aspect ratio nanofeatured surfaces with electroless deposition to produce an integrated nickel current collector followed by physical vapor deposition of a silicon layer to form a high capacity silicon anode. This composite silicon anode produced high capacities (3300 mAh/g), excellent charge—discharge cycling stability (0.20% loss per cycle at 1C), and consistent rate capabilities (46.4% at 4C) between 0 and 1.5 V. The biological templated nanocomposite electrode architecture displays a nearly 10-fold increase in capacity over currently available graphite anodes with remarkable cycling stability.

KEYWORDS: silicon anode · lithium-ion battery · Tobacco mosaic virus · physical vapor deposition · nanostructure

Silicon has emerged as one of the most promising next-generation anode materials for lithium-ion batteries due to its high theoretical capacity of 3572 mAh/g per weight and 8322 mAh/cm^3 per volume for $Li_{3.75}Si$ at room temperature.[1,2] Despite its high capacity, however, the extreme volume change, 300−400%,[3] during lithium insertion and extraction leads to severe particle pulverization, resulting in electrically disconnected silicon particles and rapid capacity fading.[4] Recently, silicon nanowires and nanotubes have been used to produce stable silicon anodes.[4−11] The architecture of these nanowires and tubes allows for a greater level of expansion to accommodate the volume changes that accompany silicon charge and discharge cycles. This architecture also endows the silicon anode with a capacity of more than 2000 mAh/g at 0.2C and 0.1−1.0 V cycling. At a 1C cycling current, carbon−silicon core−shell anodes can still provide 800 mAh/g and maintain this capacity for 80 cycles.[8] The cycling stability and rate capability of nanostructured silicon electrodes can be improved if an electronically conductive core could be directly patterned on the current collector substrate without the use of binders.[5]

There is a growing interest in harnessing the self-assembly and inorganic binding capabilities derived from biological materials for use in device and energy-storage development. In particular, the genetic tractability of viruses has been exploited to develop novel bioinorganic interfaces.[12−15] Using these novel interfaces, viruses have been structured into conductive nanowires, transistors, memory devices, and battery electrode materials.[16−20] Our team has developed Tobacco mosaic virus (TMV) as a novel bioinorganic template that can be easily patterned on metal substrates to form nanoscaled three-dimensional (3-D) structures.[14]

The TMV is a high aspect ratio cylindrical plant virus with a length of 300 nm, an outer diameter of 18 nm, and an inner diameter of 4 nm. Genetically modifying the virus to introduce cysteine residues (amino acids with thiol groups) in its coat protein enables patterning of the TMV onto metal surfaces as well as enhanced metal coating in electroless plating solutions due to strong covalent-like interactions between the thiol groups of the cysteines and metal ions.[21] In previous work, we have utilized the TMV1cys (an engineered virus containing one exposed cysteine residue per coat protein subunit yielding ~2100 cysteine residues per virus particle) for the synthesis of nickel and cobalt nanowires. These structures self-assemble vertically onto gold substrates due to the surface exposure of cysteine-derived thiol groups at the 3′ end of the TMV rod.[14] Virus-assembled nanofeatures produced a 13−80-fold increase in reactive surface area depending upon virus concentration.[14] Incorporation of these surfaces into simple nickel−zinc microbatteries also improved performance compared to planar electrode geometries.[14,22]

*Address correspondence to cswang@umd.edu.

Received for review May 4, 2010 and accepted August 5, 2010.

Published online August 13, 2010. 10.1021/nn100963j

In this study, we demonstrate that metal coatings on patterned 3-D TMV1cys templates can be used as a substrate to fabricate multilayered nanoscale 3-D silicon anodes with the internal metal layer functioning as a strong current collector. Unlike previously reported methodologies that have utilized biological templates for the synthesis of nanomaterials and relied on powder mixing and ink casting for the electrode fabrication,[16] the method presented in this study involves the direct fabrication of a nanostructured silicon electrode. Every silicon nanowire is connected to the patterned current collector, and as a result, the need for binders or conducting additives, which add extra weight, is eliminated. This TMV1cys-structured electrode enables excellent rate capability due to the high electrical conductivity of the inner metal layer within each silicon nanowire. The simplicity in fabricating electrodes combined with the biorenewable nature of the TMV1cys template as well as the potential to integrate this technique into large-scale batch manufacturing processes[23] makes this approach a promising alternative for the realization of next-generation anodes for lithium-ion batteries.

TMV1cys/Ni/Si anodes were fabricated by vertically aligning the 300 × 18 nm TMV1cys virus on the stainless steel current collector (*via* genetically engineered coat protein cysteine residues), followed by chemical deposition of nickel in an electroless plating bath to form a 3-D current collector, and finally silicon physical vapor deposition (PVD). The synthesis process of the silicon anode is shown schematically in Figure 1 and consists of four steps. It begins with the TMV1cys self-assembly (step 1), during which precleaned stainless steel disks (15.5 mm in diameter) are immersed in a TMV1cys solution with a concentration of 0.1 g/L in 0.1 M sodium phosphate buffer, pH 7, for 48 h to allow confluent virus attachment across the entire disk surface. Specifically, the 1cys genetic modification is surface-accessible only at the 3′ end of the virus rod. This configuration promotes the near-vertical attachment of the virus rod to the rough stainless steel surface. Step 2 involves the activation of the surface-assembled TMV1cys with palladium catalytic clusters *via* the reduction of Pd^{2+} to Pd^0 on the exposed cysteine residues using a hypophosphite reducing agent.[14] Following this process, nickel is deposited on the Pd^0 activated virus surface in an electroless plating solution (step 3).[14] Activated TMV1cys templates are put into a 0.1 M $NiCl_2$ plating solution for 5 min with the addition of 0.5 M $(CH_3)_2NHBH_3$ (dimethylamine borane, DMAB) as a reducing agent. After nickel deposition, the samples were dried overnight in a vacuum oven at 120 °C to evaporate any water left on the surface and avoid oxidation. After fabricting the patterned TMV1cys/Ni current collector, PVD in an AJA sputtering system (AJA international, Inc.) is used to realize the silicon anode. The process is performed in RF mode with a power of 200 W,

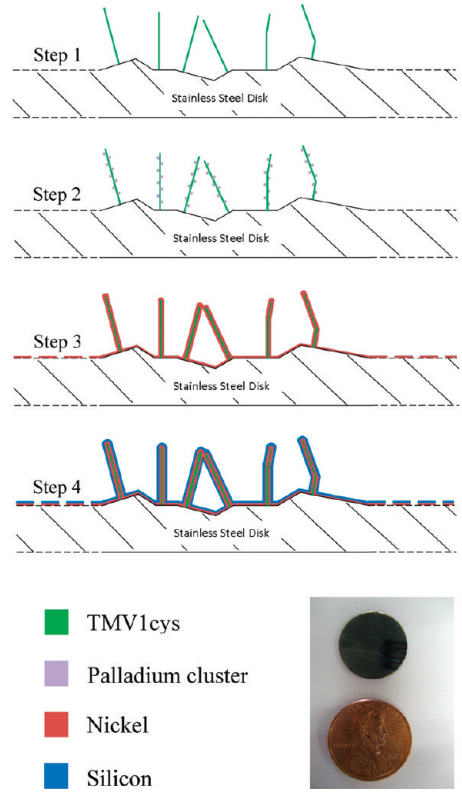

Figure 1. Diagram for the assembly of nickel-coated TMV1cys templates attached to a stainless steel surface, silicon deposition onto templates, and a picture of an assembled electrode.

an argon gas flow of 20 sccm, and a chamber pressure of 5 mTorr. The distance between the silicon target and the virus-coated steel disk substrates was set to approximately 110 mm, and the chuck was rotated to achieve better uniformity. An optical image of the assembled and fully coated anode is presented in Figure 1. To estimate the silicon loading, the parameter of interest for capacity calculations, the mass of each disk was weighed with a high-precision microbalance (Mettler Toledo, XS105 dualRange) with an accuracy of 1 μg both before and after silicon deposition. The electrochemical performance of the TMV1cys-structured anode was evaluated in a half-cell configuration. TMV1cys/Ni/Si-coated disks are assembled into coin cells (R2032) in an argon-filled glovebox, using lithium foil as a counter electrode and a 1 M $LiPF_6$ solution in ethylene carbonate/diethyl carbonate (1:1 by volume) as electrolyte. Before cell assembly in the argon-filled glovebox, the TMV1cys/Ni/Si-coated disks are annealed at 350 °C for 1 h in the glovebox to remove the moisture and other impurities that are absorbed onto nickel and silicon. An Arbin BT-2000 battery test system with computer-operated software was used to conduct the experiments and record the data.

Figure 2 shows SEM images of nickel-coated TMV1cys before and after silicon deposition for 1.0 h. In Figure 2a, most TMV1cys attach on the stainless steel surface vertically or near-vertically due to the surface

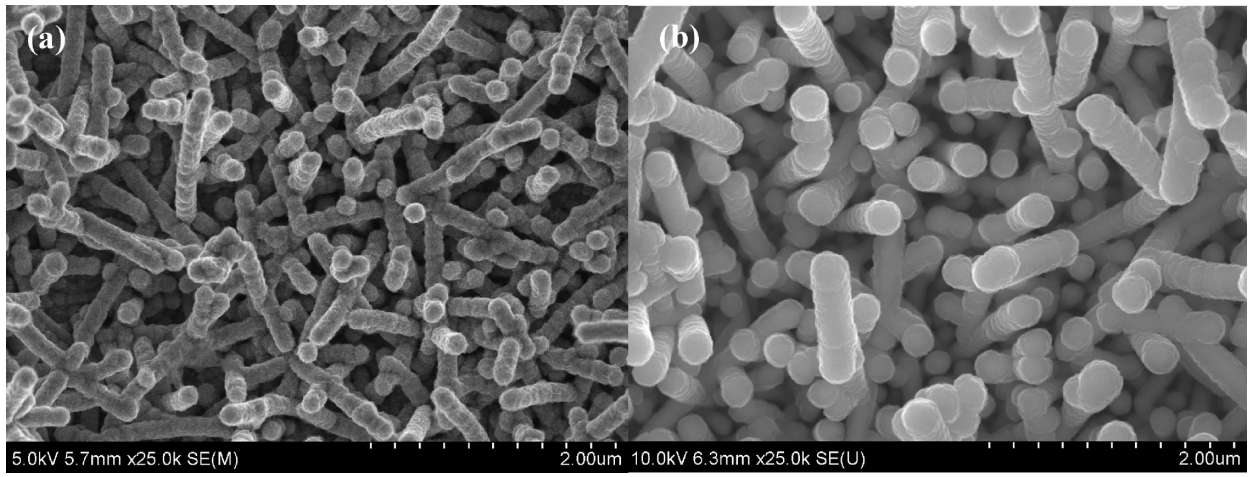

Figure 2. SEM image (a) before and (b) after silicon deposition.

roughness. Few TMV1cys lay down on stainless steel because there is clearly some flexibility in this attachment and in the virus rods themselves when the virus rods are attached to the rough surface from one end.[14] Due to the self-alignment of two or three TMV1cys particles in the assembly process, the length of surface-attached TMV1cys rods varies from 300 nm for a single TMV1cys to 900 nm for three aligned TMV1cys.[14] On the basis of the metal coating thickness L from previous work (20−40 nm),[14] the average length of nickel-coated TMV1cys rod is $\sim 600 + L \pm 300$ nm. Coated surfaces remained stable even after vigorous rinsing to remove excess plating solution. After silicon deposition, the final diameter of the TMV1cys was ~300 nm after 1.0 h silicon PVD (Figure 2b). Since nickel and silicon were coated both on the top and on the side of *the particle*, the final TMV1cys/Ni/Si rods have a length of $\sim 750 \pm 300$ nm and a diameter of ~300 nm, which make the rods retain their columnar structure after nickel and silicon coatings.

Figure 3 displays TEM and fast Fourier transform (FFT) images of a single virus rod consisting of two aligned TMV1cys, nickel, and silicon layers after 45 min of silicon PVD. The TMV1cys and the nickel and silicon layers are clearly visible in Figure 3a,d. The high-resolution TEM (HRTEM) and FFT images clearly show that the silicon is amorphous.[24] The innermost structure is the rod-shaped TMV1cys with a diameter of 18 nm, which explains why the intensity of the EDS spectrum decreases in this region for both nickel and silicon. A nickel metal layer with 38 nm thickness uniformly covers the entire TMV1cys outer surface. Our previous studies demonstrated that these nickel coatings also fully covered the attachment point of the particle to the metal substrate,[14] forming a continuous 3-D-patterned Ni current collector. The outermost layer is the silicon-sputtered material, which has a similar thickness of 38 nm. Silicon layer uniformity obtained *via* PVD depends upon the relative orientation of the virus particles. Viruses assembled onto the current collector were near-vertically oriented as previously described.[14] This alignment results in near-uniform silicon coatings (Figure 3a) for near-vertical orientation, which has only a slight thickening of silicon (Figure 3d) detectable on the upper sections of the assembled viruses for nonvertical TMV1cys. In both cases, however, TEM images indicate

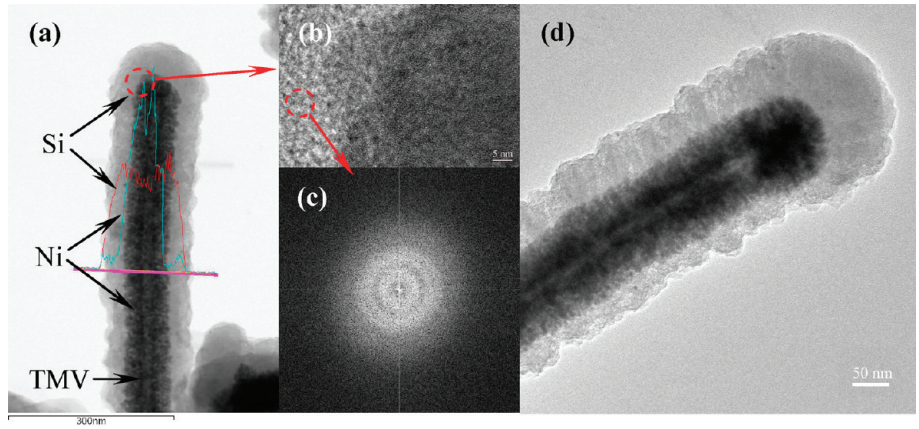

Figure 3. (a) TEM image of a vertical TMV1cys/Ni/Si nanowire after 45 min of silicon PVD, including EDS profiles of nickel and silicon. (b) HRTEM image of circled area in (a). (c) FFT image of silicon layer and (d) nonvertical TMV1cys/Ni/Si nanowires after 45 min of silicon PVD.

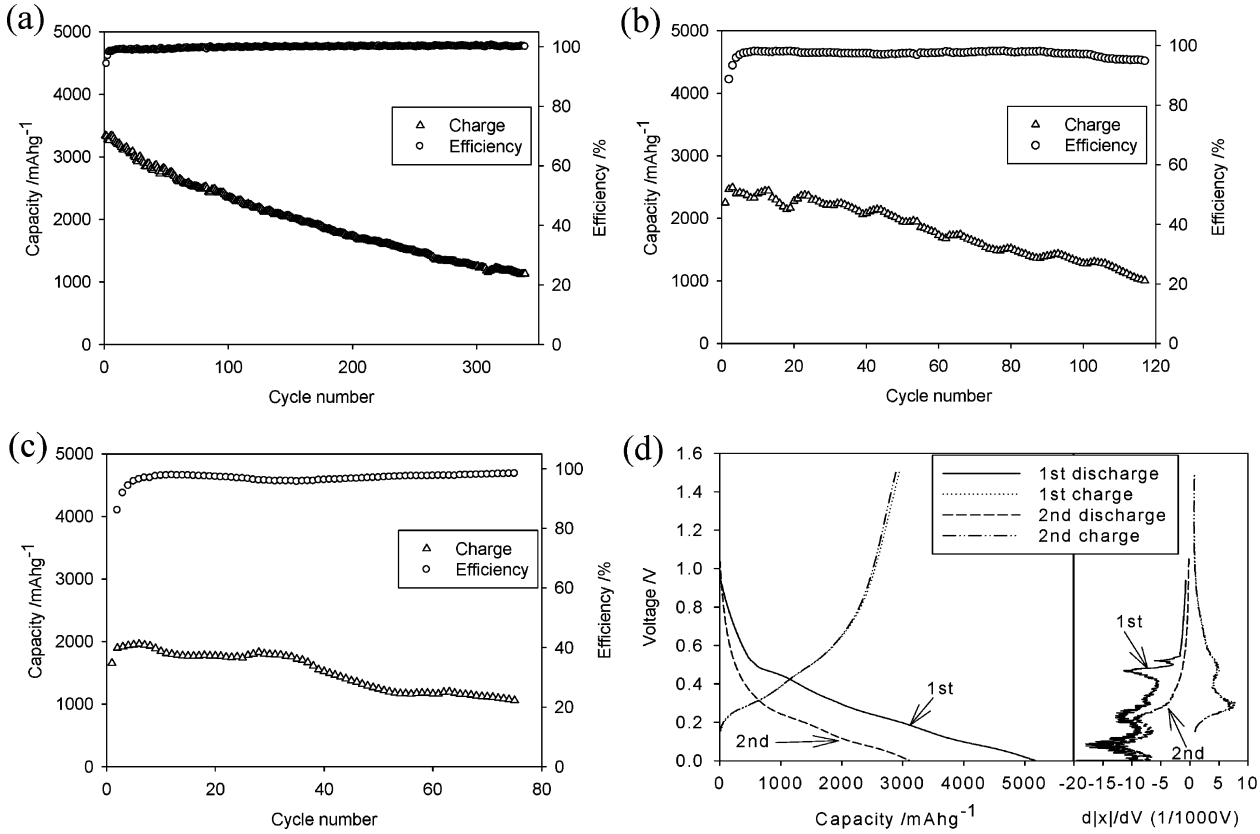

Figure 4. Cyclic performance of the 3-D TMV1cys/Ni/Si anode at (a) 1C, (b) 2C, (c) 4C, and (d) charge−discharge profiles with differential capacity curves at 1C (1C = 2000 mA/g) after being annealed at 350 °C for 1 h in argon atmosphere. The capacity calculation is based on the weight of the active material, silicon.

that for every silicon nanowire there is a nickel core that directly connects it to the stainless steel disk current collector. This novel 3-D nanoarchitecture allows the coated silicon shell to maintain a direct electrical connection along the entire length of the virus-templated nanowire.

Anodes sputter coated for 45 min were assembled in coin cells against a lithium foil and tested for their cyclic ability at room temperature (~25 °C). The silicon loading on each electrode is approximately 50 μg. Figure 4 shows capacity retention of a silicon anode charged and discharged between 0 and 1.5 V at specific *C* rates (tests were terminated upon reaching a capacity of less than 1000 mAh/g). These graphs plot the anode charge capacities as well as its Coulombic efficiency, defined as the ratio of the charge to discharge capacities. The Coulombic efficiencies approach 100% after 5 to 6 cycles for all *C* rates. As indicated in Figure 4, the average fading rate is 0.20% per cycle for 1C, 0.46% per cycle for 2C, and 0.50% per cycle for 4C. The discharge capacity during the second cycle is 3343 mAh/g at 1C, 2251 mAh/g at 2C, and 1656 mAh/g at 4C. Compared to previously reported values for silicon and carbon/silicon nanowires,[4−10] the TMV1cys-enabled silicon anode presented here combines high capacity (up to 3343 mAh/g at 1C), low fading rate (as low as 0.20% per cycle at 1C), and excellent charge−discharge ability (1656 mAh/g at 4C) for a large number of operating cycles. As discussed previously, this remarkable cyclic ability can be attributed to the unique multilayer nanostructure of the anode, specifically the highly conductive nickel layer encased by nanolayer coatings of silicon for direct current collection. In addition to the core−shell structure, the very thin layer (40 nm) of amorphous silicon also contributed greatly to the charge/discharge cycling stability. Graetz *et al.* reported that amorphous silicon nanofilms were much more robust compared to nanocrystalline silicon films during electrochemical cycling.[25] This core−shell structure allows charging at higher *C* rates with a higher capacity and stability than previously reported silicon nanowires that have a similar structure but require a low *C* rate charging (0.2C) to achieve a high capacity.[4−7] For the TMV1cys-structured silicon anode presented here, it takes about 340 cycles at 1C, 120 cycles at 2C, and 75 cycles at 4C to reach the capacity retention of 1000 mAh/g.

The first and second charge−discharge profiles of a TMV1cys-enabled silicon anode at 1C are shown in Figure 4d, along with the differential capacity curves. The irreversible capacity in the first cycle is around 40%. On the basis of the EDS spectrum, the atomic ratio of silicon, nickel, and oxygen is 44:27:29. The oxygen is induced during the nickel electroless deposition and

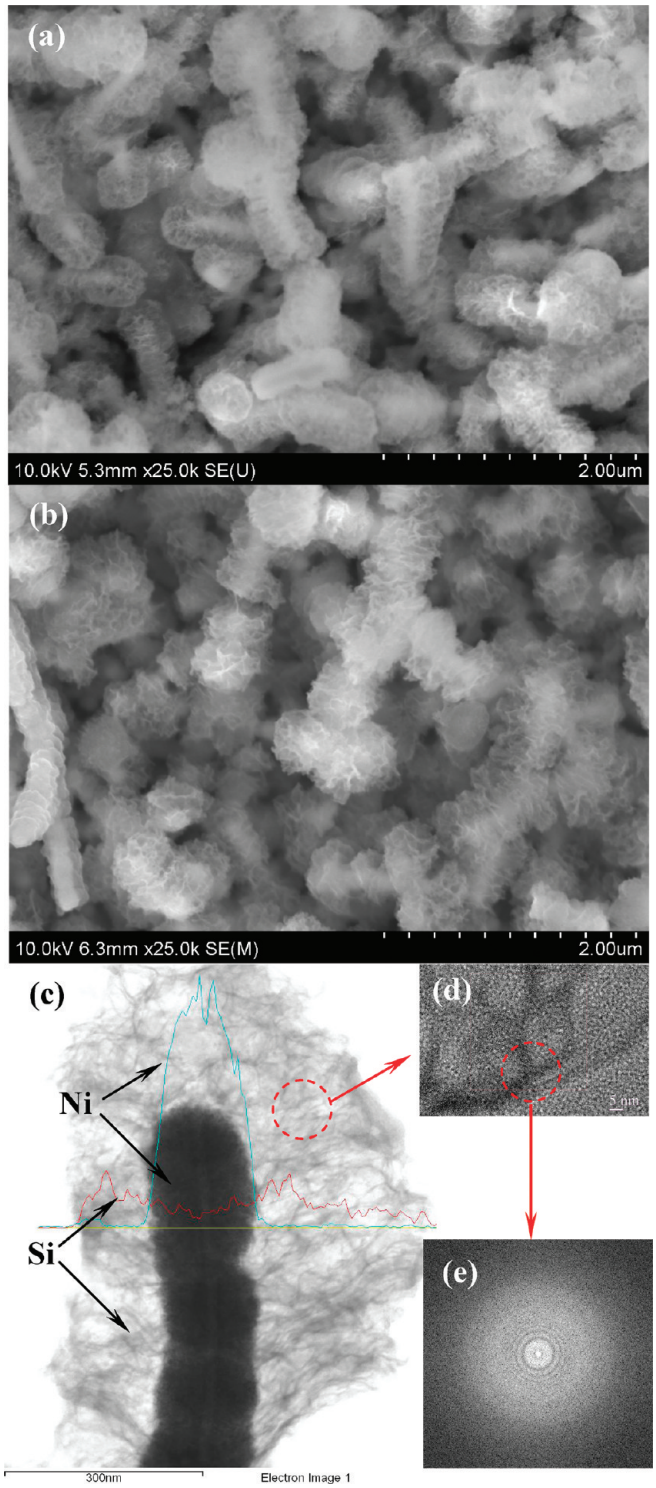

Figure 5. Occurrence of a sponge-like silicon morphology upon cycling. SEM images of TMV1cys/Ni/Si electrodes after 35 (a) and 75 (b) cycles at 1C. (c) TEM image with EDS spectra for nickel and silicon after 75 cycles at 1C. (d) HRTEM image of silicon after 75 cycles. (e) FFT image of silicon after 75 cycles.

sample transportation. Most oxygen exists in the forms of SiO_x, which can react with lithium ($SiO_x + 2xLi \rightleftarrows Si + xLi_2O$). This reaction is partially reversible, and the reversibility depends on the x value.[26,27] Thus, the combination of SiO_x reduction and SEI formation in the first discharge accounts for the irreversible capacity.[28−32] The bare TMV1cys does not react with lithium in electrolyte in the potential range from 0.0 to 1.5 V, as confirmed by a control experiment using the uncoated TMV1cys as a working electrode and lithium film as a counter electrode (data not shown). The differential capacity curves of the TMV1cys/Ni/Si anode in Figure 4d showed a typical amorphous silicon charge−discharge behavior.[33,34] Peaks between 0.4 and 0.6 V in the first discharge process contribute to the side reaction related to SEI film formation and disappear in the second discharge process. Two peaks at ~0.23 and ~0.1 V during discharge and two peaks at ~0.3 and ~0.45 V during charge in Figure 4d are consistent with reported differential capacity curves of thin amorphous silicon layers.[34,35]

The silicon anode structure after 35 and 75 cycles at 1C rate was examined to investigate degradation mechanisms on the virus-structured nanowires. Prior to disassembling the coin cell, a constant voltage of 1.5 V was applied on the silicon electrodes for a period of 48 h to completely extract lithium from the silicon. Shown in Figure 5 are SEM images after 35 (a) and 75 (b) cycles of operation. A porous sponge-like silicon structure developed during repeated lithium insertions and extractions, as evidenced by the SEM images before cycling (Figure 2b), after 35 cycles (Figure 5a), and after 75 cycles (Figure 5b). This observation suggested that the volume of silicon gradually increased during the charge/discharge cycles. The delithiated silicon layer expanded from 38 nm (Figure 3a) to 150 nm (Figure 5c) in thickness after 75 charge/discharge cycles. Previous reports indicate that silicon volume expands ~3-fold after full lithiation at room temperature.[36] The volume of the delithiated porous sponge-like silicon layer on the virus-enabled anode was still 3−4 times greater than the volume of the silicon layer prior to lithiation (Figures 5c and 3a). This observation suggests that once the volume of the sponge-like silicon layer has expanded it is not reversible, which greatly enhanced the cycling stability of TMV1cys/Ni/Si anodes. As demonstrated in Figure 5c, after expansion, silicon shell coatings remain connected to the conductive nickel core. The mechanical integrity between silicon, nickel, and the surface-mounted virus proved to be highly resistant to the stresses associated with silicon expansion. Therefore, the increased silicon volume combined with the mechanical integrity of the TMV1cys/Ni/Si surface likely accounts for the observed cycling stability of this anode. The HRTEM image in Figure 5d and the FFT image in Figure 5e demonstrate that the silicon still remains amorphous after 75 charge/discharge cycles. The fiber-like structure in Figure 5c,d is most likely induced by the different density of the porous silicon.

The expanded volume of the sponge-like silicon layer is expected to increase the available surface area and enhance the electrochemical reactions. To examine

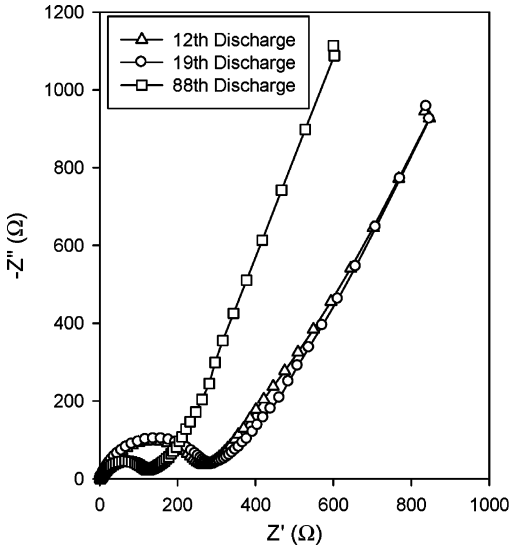

Figure 6. Impedance investigations after the 12th, 19th, and 88th discharge to 0.0 V followed by 2.0 h of rest in an open-circuit potential. The depressed semicircle in the high-frequency region is attributed to the overlap between the SEI impedance and charge transfer impedance.

the effects of the sponge-like silicon layer on the electrochemical performance, the charge/discharge kinetics of the anode were analyzed using electrochemical impedance spectroscopy. Figure 6 shows the impedance of TMV1cys/Ni/Si anodes at the 12th, 19th, and 88th cycles. All of the impedance spectra have similar features: a medium-to-high frequency depressed semicircle and an inclined low-frequency line, a behavior that is in good agreement with previously reported impedance spectra for silicon nanowires.[7] The inclined line in the low-frequency region represents the lithium diffusion impedance,[37] while the depressed semicircle is attributed to the overlap between the SEI film and the interfacial charge transfer impedance.[7] Impedance studies revealed that the total SEI and charge transfer resistances slightly increase at first and then decrease after the 19th cycle. SEM images of the TMV1cys/Ni/Si anodes demonstrated that the sponge-like silicon structures were formed by the 35th cycle and were fully developed by the 75th cycle. These findings suggest that the observed sponge-like silicon layer is responsible for the enhanced reaction kinetics.

In most cases when silicon nanowires have been used as anode materials, silicon stability and improvements in cycling stability are achieved by using higher discharge (lithiation) cutoff voltages of 10 to 150 mV[3−9] as a means to avoid the inhomogeneous and detrimental volume changes that occur between amorphous and crystalline silicon at ~60 mV.[38] In this work, TMV1cys-structured anodes were cycled between 0.0 and 1.5 V without significantly compromising the stability of the silicon anode. The high capacity obtained from this anode, even at a 0.0 V cutoff limit, is an indication of the robustness of the synthesized virus-based materials.

In summary, the TMV1cys-enabled silicon anode reported here has a novel 3-D nanostructure. The macromolecular structure of the TMV1cys functions as a nanoscale scaffold for the assembly of a nickel conducting core that provides the support for the deposition of the silicon-sputtered anode material as well as a highly conductive matrix connecting the surface of the nanowires to the steel current collector. After more than 340 cycles between 0.0 and 1.5 V at 1C, more than 1100 mAh/g capacity remained. Interestingly, a sponge-like silicon structure formed after repeated charge/discharge cycles enhances both reaction kinetics and anode stability. These results, combined with the simplicity of the TMV1cys self-assembly and patterning process (neutral pH, room temperature), represent a new strategy for the development of inexpensive and versatile synthesis techniques for energy-storage applications.

Acknowledgment. The authors acknowledge financial support from the Department of Energy (DESC0001160) under the project science of precision multifunctional nanostructures for electrical energy storage and Maryland Technology Development Corporation (TEDCO 09102380), and the technical support of the Maryland NanoCenter. J.N.C. also acknowledges the support of the Department of Energy, the Office of Basic Energy Sciences DEFG02-02-ER45975.

REFERENCES AND NOTES

1. Boukamp, B. A.; Lesh, G. C.; Huggins, R. A. All-Solid Lithium Electrodes with Mixed-Conductor Matrix. *J. Electrochem. Soc.* **1981**, *128*, 725–729.
2. Cahen, S.; Janot, R.; Laffont-Dantras, L.; Tarascon, J. M. Chemical Reduction of $SiCl_4$ for the Preparation of Silicon−Graphite Composites Used as Negative Electrodes in Lithium-Ion Batteries. *J. Electrochem. Soc.* **2008**, *155*, A512–A519.
3. Kasavajjula, U.; Wang, C.; Appleby, A. J. Nano- and Bulk-Silicon-Based Insertion Anodes for Lithium-Ion Secondary Cells. *J. Power Sources* **2007**, *163*, 1003–1039.
4. Chan, C. K.; Peng, H.; Liu, G.; Mcllwrath, K.; Zhang, X.; Huggins, R. A.; Cui, Y. High-Performance Lithium Battery Anodes Using Silicon Nanowires. *Nat. Nanotechnol.* **2008**, *3*, 31–35.
5. Chan, C. K.; Ruffo, R.; Hong, S. S.; Huggins, R. A.; Cui, Y. Structural and Electrochemical Study of the Reaction of Lithium with Silicon Nanowires. *J. Power Sources* **2009**, *189*, 34–39.
6. Cui, L.; Ruffo, R.; Chan, C. K.; Peng, H.; Cui, Y. Crystalline-Amorphous Core−Shell Silicon Nanowires for High Capacity and High Current Battery Electrodes. *Nano Lett.* **2009**, *9*, 491–495.
7. Ruffo, R.; Hong, S. S.; Chan, C. K.; Huggins, R. A.; Cui, Y. Impedance Analysis of Silicon Nanowire Lithium Ion Battery Anodes. *J. Phys. Chem. C* **2009**, *113*, 11390–11398.
8. Cui, L.; Yang, Y.; Hsu, C.; Cui, Y. Carbon−Silicon Core−Shell Nanowires as High Capacity Electrode for Lithium Ion Batteries. *Nano Lett.* **2009**, *9*, 3370–3374.
9. Kim, H.; Cho, J. Superior Lithium Electroactive Mesoporous Si@Carbon Core−Shell Nanowires for Lithium Battery Anode Material. *Nano Lett.* **2008**, *8*, 3688–3691.
10. Peng, K.; Jie, J.; Zhang, W.; Lee, S. Silicon Nanowires for Rechargeable Lithium-Ion Battery Anodes. *Appl. Phys. Lett.* **2008**, *93*, 033105.
11. Park, M.-H.; Kim, M. G.; Joo, J.; Kim, K.; Kim, J.; Ahn, S.; Cui, Y.; Cho, J. Silicon Nanotube Battery Anodes. *Nano Lett.* **2009**, *9*, 3844–3847.
12. Fowler, C. E.; Shenton, W.; Stubbs, G.; Mann, S. Tobacco Mosaic Virus Liquid Crystals as Templates for the Interior

Design of Silica Mesophases and Nanoparticles. *Adv. Mater.* **2001**, *13*, 1266–1269.
13. Dujardin, E.; Peet, C.; Stubbs, G.; Culver, J. N.; Mann, S. Organization of Metallic Nanoparticles Using Tobacco Mosaic Virus Templates. *Nano Lett.* **2003**, *3*, 413–417.
14. Royston, E.; Ghosh, A.; Kofinas, P.; Harris, M. T.; Culver, J. N. Self-Assembly of Virus-Structured High Surface Area Nanomaterials and Their Application as Battery Electrodes. *Langmuir* **2008**, *24*, 906–912.
15. Shenton, W.; Douglas, T.; Young, M.; Stubbs, G.; Mann, S. Inorganic−Organic Nanotube Composites from Template Mineralization of Tobacco Mosaic Virus. *Adv. Mater.* **1999**, *11*, 253–256.
16. Nam, K. T.; Kim, D. W.; Yoo, P. J.; Chiang, C. Y.; Meethong, N.; Hammond, P. T.; Chiang, Y. M.; Belcher, A. M. Virus-Enabled Synthesis and Assembly of Nanowires for Lithium Ion Battery Electrodes. *Science* **2006**, *312*, 885–888.
17. Lee, S. Y.; Choi, J. W.; Royston, E.; Janes, D. B.; Culver, J. N.; Harris, M. T. Deposition of Platinum Clusters on Surface-Modified Tobacco Mosaic Virus. *J. Nanosci. Nanotechnol.* **2006**, *6*, 974–981.
18. Tseng, R. J.; Tsai, C. L.; Ma, L. P.; Ouyang, J. Y.; Ozkan, C. S.; Yang, Y. Digital Memory Device Based on Tobacco Mosaic Virus Conjugated with Nanoparticles. *Nat. Nanotechnol.* **2006**, *1*, 72–77.
19. Keren, K.; Berman, R. S.; Buchstab, E.; Sivan, U.; Braun, E. DNA-Templated Carbon Nanotube Field-Effect Transistor. *Science* **2003**, *302*, 1380–1382.
20. Lee, Y. J.; Yi, H.; Kim, W.-J.; Kang, K.; Yun, D. S.; Strano, M. S.; Ceder, G.; Belcher, A. M. Fabricating Genetically Engineered High-Power Lithium-Ion Batteries Using Multiple Virus Genes. *Science* **2009**, *324*, 1051–1055.
21. Lee, S.; Royston, E.; Culver, J. N.; Harris, M. T. Improved Metal Cluster Deposition on a Genetically Engineered Tobacco Mosaic Virus Template. *Nanotechnology* **2005**, *16*, S435–S441.
22. Gerasopoulos, K.; McCarthy, M.; Royston, E.; Culver, J. N.; Ghodssi, R. Nanostructured Nickel Electrodes Using the Tobacco Mosaic Virus for Microbattery Applications. *J. Micromech. Microeng.* **2008**, *18*, 104003.
23. Gerasopoulos, K.; McCarthy, M.; Banerjee, P.; Fan, X.; Culver, J. N.; Ghodssi, R. Biofabrication Methods for the Patterned Assembly and Synthesis of Viral Nanotemplates. *Nanotechnology* **2010**, *21*, 055304.
24. Shim, J.; Cho, N.; Kim, J.; Kim, Y. Formation of Si Nanocrystallites in Al-Added Amorphous Si Films by Electron Beam Irradiation. *Jpn. J. Appl. Phys.* **2010**, *49*, 035001.
25. Graetz, J.; Ahn, C. C.; Yazami, R.; Fultz, B. Highly Reversible Lithium Storage in Nanostructured Silicon. *Electrochemical and Solid-State Letters* **2003**, *6*, A194–A197.
26. Su, L.; Zhou, Z.; Ren, M. Core Double−Shell Si@SiO_2@C Nanocomposites as Anode Materials for Li-Ion Batteries. *Chem. Commun.* **2010**, *46*, 2590–2592.
27. Kim, H.; Seo, M.; Park, M.; Cho, J. A Critical Size of Silicon Nano-Anodes for Lithium Rechargeable Batteries. *Angew. Chem., Int. Ed.* **2010**, *49*, 2146–2149.
28. Wachtler, M.; Besenhard, J. O.; Winter, M. Tin and Tin-Based Intermetallics As New Anode Materials for Lithium-Ion Cells. *J. Power Sources* **2001**, *94*, 189–193.
29. Yang, S.; Zavalij, P. Y.; Whittingham, M. Anodes for Lithium Batteries: Tin Revisited. *Electrochem. Commun.* **2003**, *5*, 587–590.
30. Wagner, M. R.; Raimann, P. R.; Trifonova, A.; Moeller, K.-C.; Besenhard, J. O.; Winter, M. Electrolyte Decomposition Reactions on Tin- and Graphite-Based Anodes are Different. *Electrochem. Solid-State Lett.* **2004**, *7*, A201–A205.
31. Menkin, S.; Golodnitsky, D.; Peled, E. Artificial Solid-Electrolyte Interphase (SEI) for Improved Cyclability and Safety of Lithium-Ion Cells for EV Applications. *Electrochem. Commun.* **2009**, *11*, 1789–1791.
32. Lucas, I. T.; Pollak, E.; Kostecki, R. *In Situ* AFM Studies of SEI Formation at a Sn Electrode. *Electrochem. Commun.* **2009**, *11*, 2157–2160.
33. Obrovac, M. N.; Krause, L. J. Reversible Cycling of Crystalline Silicon Powder. *J. Electrochem. Soc.* **2007**, *154*, A103.
34. Hatchard, T. D.; Dahn, J. R. *In Situ* XRD and Electrochemical Study of the Reaction of Lithium with Amorphous Silicon. *J. Electrochem. Soc.* **2004**, *151*, A838.
35. Wang, W.; Kumta, P. N. Nanostructured Hybrid Silicon/Carbon Nanotube Heterostructures: Reversible High-Capacity Lithium-Ion Anodes. *ACS Nano* **2010**, *3*, 2233.
36. Beattie, S. D.; Larcher, D.; Morcrette, M.; Simon, B.; Tarascon, J.-M. Si Electrodes for Li-Ion Batteries—A New Way to Look at an Old Problem. *J. Electrochem. Soc.* **2008**, *155*, A158.
37. Wang, C.; Appleby, A. J.; Little, F. E. Charge-Discharge Stability of Graphite Anodes for Lithium-Ion Batteries. *J. Electroanal. Chem.* **2001**, *497*, 3–46.
38. Li, J.; Dahn, J. R. An *In Situ* X-ray Diffraction Study of the Reaction of Li with Crystalline Si. *J. Electrochem. Soc.* **2007**, *154*, A156–A161.